CrystEngComm

PAPER

View Article Online
View Journal | View Issue

Cite this: *CrystEngComm*, 2018, **20**, 6077

A stable polyoxometalate-based porous coordination polymer with high proton conductivity†

Yu-Hui Luo,[ab] Li-Qiang Yi,[b] Jia-Ni Lu,[a] Long-Zhang Dong[a] and Ya-Qian Lan*[a]

Received 29th April 2018,
Accepted 14th August 2018

DOI: 10.1039/c8ce00693h

rsc.li/crystengcomm

A new coordination polymer based on the Keggin-type $[SiW_{12}O_{40}]^{4-}$, namely, $[Cu_4L_2(SiW_{12}O_{40})(OH)_4(H_2O)_8]\cdot8H_2O$ (**1**), has been prepared by a hydrothermal method (L = 1,4-bis(4*H*-1,2,4-triazol-4-yl)benzene). The supramolecular framework of **1** is constructed from two dimensional Cu–L layers. Compound **1** was found to be stable in aqueous solutions having pH values ranging from 1 to 13 as well as some other boiling solvents, such as boiling water, methanol and ethanol. Compound **1** exhibits a proton conductivity of 1.4×10^{-4} S cm^{-1} at 65 °C and 98% RH. More importantly, the proton conductivity of **1** presents a 28-fold enhancement (3.9×10^{-3} S cm^{-1} at 65 °C and 98% RH) by immersing its gourd-shaped channels into $N_2H_4\cdot H_2SO_4$.

Introduction

Proton-exchange membrane fuel cells (PEMFCs) have attracted increasing attention due to their highly stable and efficient energy conversion with ultralow emission.[1–5] To date, the most widely used proton-exchange membrane (PEM) is a perfluorinated PEM (*e.g.* Nafion). However, the operating condition restriction and high cost limit its applications.[6] Hence, the design and synthesis of new solid proton conductors are enormously important for energy conversion applications.

Coordination polymers (CPs), a class of compounds with highly tunable structures, have recently been proven as good candidate materials for proton conduction to replace the existing PEM in fuel cells.[7–10] The two important structural characteristics of proton-conducting CPs are proton carriers (*e.g.* water, imidazole and sulfonic groups) and proton-conducting pathways (*e.g.* hydrogen-bond networks).[11–17] The modifiable network and channel environment of CPs allow these structural bases to be controlled and thereafter their proton conductivity. Polyoxometalates (POMs), a large family of metal–oxygen clusters with an oxygen-rich surface can supply more proton transfer sites to construct unobstructed hydrogen-bond networks.[18–26] With these in mind, we have designed several types of POM-based CPs with more favourable proton-conducting properties.[27,28] In our previous work, small N-containing aromatic heterocyclic ligands were used for they not only could provide more protons, but also could form π–π stacking. Both of these structural characteristics can help construct proton transfer passages.[27] Herein, we choose 1,4-bis(4*H*-1,2,4-triazol-4-yl)benzene (L), whose size matches with those of Keggin-type POMs, as a N-donor ligand to construct new POM-based CPs. A new porous coordination polymer based on Keggin-type $[SiW_{12}O_{40}]^{4-}$ (SiW_{12}) has been obtained, namely, $[Cu_4L_2(SiW_{12}O_{40})(OH)_4(H_2O)_8]\cdot8H_2O$ (**1**). The supramolecular framework of **1** was constructed from two-dimensional (2D) Cu–L layers. Stability studies reveal that compound **1** not only can retain its intact structure in aqueous solutions with pH ranging from 1 to 13, but also can be stable in boiling solvents, such as water, methanol and ethanol. Compound **1** shows a proton conductivity of 1.4×10^{-4} S cm^{-1} at 65 °C and 98% RH. Interestingly, compound **1a**, which is formed by immersing **1** in a $N_2H_4\cdot H_2SO_4$ solution, presents a proton conductivity of up to 3.9×10^{-3} S cm^{-1} at 65 °C and 98% RH, which is 28 times higher than that of **1**.

Experimental

Materials and general methods

All reagents and solvents were purchased from commercial sources and used without further purification. Powder X-ray diffraction (PXRD) patterns were collected on a Rigaku SmartLab X-ray diffractometer with graphite monochromatized Cu Kα radiation (λ = 0.15418 nm) and 2θ ranging from 5 to 50°. The FT-IR spectra were measured in KBr pellets in the range 4000–400 cm^{-1} on a Bruker VERTEX70 spectrometer. Elemental analysis (EA) for C, H and N was

---

[a] School of Chemistry and Materials Science, Nanjing Normal University, Nanjing 210023, Jiangsu, P. R. China. E-mail: yqlan@njnu.edu.cn
[b] Department of Chemical Engineering, Huaihai Institute of Technology, Lianyungang 222000, Jiangsu, P. R. China

† Electronic supplementary information (ESI) available: Crystallographic information files (CIFs), other structure diagrams, Nyquist plots of **1a**, TGA curves, and tables of hydrogen bonds and selected bond lengths and angles. CCDC 1822962 (**1**). For ESI and crystallographic data in CIF or other electronic format see DOI: 10.1039/c8ce00693h

performed on a Perkin-Elmer 2400 elemental analyser. Thermogravimetric analysis (TGA) was performed on a Netzsch STA449F3 analyser with the sample heated in an Al_2O_3 crucible under a nitrogen atmosphere at a heating rate of 10 °C min^{-1}. Water vapour adsorption–desorption isotherms were measured at 298 K on a Quantachrome Instruments Autosorb AS-6B.

Synthesis of 1

A mixture of $CuCl_2 \cdot 2H_2O$ (0.1 mmol, 17.0 mg), $H_4SiW_{12} \cdot xH_2O$ (0.03 mmol, 100 mg), L (0.05 mmol, 10 mg) and H_2O (10 mL) was stirred at room temperature for 4 hours. The pH of the mixture was adjusted to about 2.0 by adding hydrochloric acid (1 mol L^{-1}). Then the mixture was transferred into a 25 mL Teflon-lined stainless-steel autoclave reactor and heated at 160 °C for 72 hours. After cooling to room temperature at a rate of 10 °C h^{-1}, blue block crystals suitable for X-ray structural analysis were isolated by ultrasonically cleaning the sample, washing with water several times and drying in air. Yield: *ca.* 35% (based on L). Anal. calcd for $C_{20}H_{52}Cu_4N_{12}O_{60}SiW_{12}$ (%): C, 6.15; H, 1.34; N, 4.30. Found: C, 6.11; H, 1.27; N, 4.24. The IR (KBr, cm^{-1}): ν = 3462(m), 3134(m), 1620(s), 1555(s), 1318(m), 1271(s), 1114(m), 1082(s), 1015(s), 969(s), 922(s), 885(s), 811(s), 636(m), 529(s).

Single-crystal X-ray crystallography

The crystal data of **1** were obtained at 296(2) K on a Bruker AXS Smart Apex CCD diffractometer with graphite-monochromated Mo-Kα radiation (λ = 0.71073 Å). The collected data were reduced as twinned, and the R_{int} value was merged. The crystal structure was solved and refined by full-matrix least-squares methods against F^2 by using SHELXS-2014 and SHELXL-2014 programs.[29] All non-hydrogen atoms were refined with anisotropic temperature parameters. All hydrogen atoms except for water molecules were placed in geometrically idealized positions using a riding model. Some of the atoms with the ADP or NDP problem were restricted by SIMU and ISOR commands. The structure refinement details and the crystallographic data for **1** are shown in Table 1.

Impedance analysis

The samples were ground into powder and then moulded into a circular pellet with a radius of 0.2 cm. The thickness of the pellets was measured using a vernier caliper. The proton conductivities were measured using an impedance/gain-phase analyzer (Solartron S1 1260) over a frequency range from 1 Hz to 1 MHz with an input voltage of 500 mV. The operation temperatures (ranging from 30 to 65 °C) and relative humidities were controlled by a constant temperature and humidity incubator. The proton conductivity was calculated using the equation $\sigma = l/SR$, where σ is the conductivity (S cm^{-1}), l is the thickness (cm) of the pellet, S is the cross-sectional area (cm^2) of the pellet and R is the bulk resistance (Ω).[8] The activation energy (E_a) was calculated from the equation $\sigma T = \sigma_0 \exp(-E_a/K_BT)$, where σ is the conductivity (S cm^{-1}), K_B is the Boltzmann constant (8.6×10^{-5} eV K^{-1}) and T is the temperature (K).[8]

Table 1 Crystal data and structure refinement for **1**

Compound	1
Empirical formula	$C_{20}H_{52}Cu_4N_{12}O_{60}SiW_{12}$
Formula weight	3909.18
Temperature	296(2) K
Wavelength	0.71073 Å
Crystal system	Monoclinic
Space group	$P2_1/c$
a	13.407(6) Å
b	20.998(9) Å
c	13.171(6) Å
β	104.296(6)°
Volume	3593(3) $Å^3$
Z	2
$F(000)$	3508
Calculated density	3.613 mg cm^{-3}
Goodness-of-fit	1.035
$R_1(wR_2)$ $[I > 2\sigma(I)]^a$	0.0802 (0.1984)

[a] $R_1 = \sum||F_0| - |F_c||/\sum|F_0|$; $wR_2 = \sum[w(F_0^2 - F_c^2)^2]/\sum[w(F_0^2)^2]^{1/2}$.

Results and discussion

Crystal structure of 1

Structural analysis indicates that **1** crystallizes in the monoclinic space group $P2_1/c$ and exhibits a porous supramolecular framework. The formula of **1** was supported by EA and TGA measurements. The Si atom of the SiW_{12} anion lies on an inversion centre, with concomitant disorder of the four oxygen atoms (O1, O2, O3, and O4) directly bonded to it. As shown in Fig. 1a, the asymmetric unit of **1** contains two crystallographically independent Cu ions, which are both six-coordinated in a distorted octahedral coordination geometry, defined by two nitrogen atoms from two L molecules, two oxygen atoms from two μ_2-OH groups and two coordination water molecules. The Cu–N bond lengths are in the range from 1.97(3) to 2.06(2) Å while the Cu–O bond lengths are in the range from 1.90(2) to 2.80(6) Å. All the copper atoms are in +2 oxidation states in compound **1**, which is confirmed by valence sum calculations (Table S4†) and coordination environments. The Cu–O bond length between Cu(II) ions and coordination water molecules is significantly longer than that between Cu(II) ions and μ_2-OH groups, since there is Jahn–Teller distortion. The Cu(II) ions are connected by μ_2-OH groups to form one-dimensional (1D) wave-shaped Cu–O–Cu chains, which are further connected by L ligands to generate 2D wavy layers (Fig. 1b, S1 and S2†). The L ligands in the 2D layer are bent into a curved shape to fabricate lots of pits on the layer surface (Fig. S3†). The SiW_{12} ions are fixed in the pits of adjacent layers by C–H⋯O hydrogen-bonding interactions to serve as pillars of the 2D layers forming a supramolecular structure (Fig. 1c and d). As viewed along the c axis, the framework of **1** contains 1D gourd-shaped channels with a widow size of 10.0 × 4.2 $Å^2$ (Fig. 1d). Moreover, the channel contains void spaces with a size of 10 × 13 × 9 $Å^3$, which are

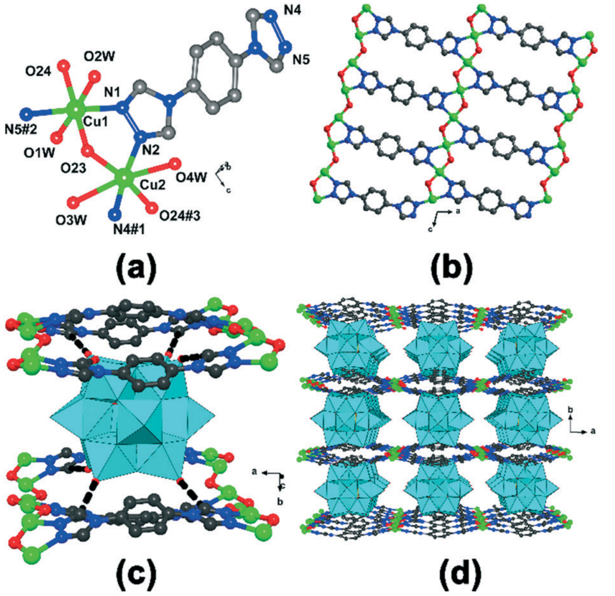

Fig. 1 (a) Coordination environments of Cu1 and Cu2 ions. Symmetry codes: #1, −1 + *x*, *y*, *z*; #2, −1 + *x*, 0.5 − *y*, −0.5 + *z*; #3, *x*, 0.5 − *y*, 0.5 + *z*. (b) View of the 2D layer of **1** constructed from L ligands connecting Cu–O–Cu chains. (c) Representation of the C–H⋯O hydrogen-bonding interaction (shown in black dashed lines) between the SiW_{12} ion and L ligands. (d) Pillar-layered structure of **1**. Color scheme: green, Cu; red, O; gray, C; blue, N; cyan polyhedron, SiW_{12}. All hydrogen atoms are omitted for clarity.

accessible to many small molecules (*e.g.* water, ammonium ion and sulfonic groups) (Fig. 2). The total potential solvent-accessible volume of **1** is calculated to be 32.7% (1173.1 Å^3 out of 3593.0 Å^3 per unit cell volume) using the PLATON program.[30]

The crystalline phase purity of compound **1** was confirmed by comparison of the measured and simulated powder X-ray diffraction (PXRD) patterns (Fig. 3). The crystals of **1** exhibit high chemical stability. No efflorescence was observed when the crystals were exposed to air over six months. Otherwise, these crystals remain intact in aqueous solutions with pH ranging from 1–13 at room temperature. They are also stable in boiling solvents such as water, methanol, and ethanol over 24 hours. TGA measurements were also carried out to investigate the thermal stability of compound **1**. The TGA curve of **1** reveals only one weight loss of 7.1% (calculated 7.4%) from 50 °C to 240 °C, caused by the loss of solvent and coordination water molecules (Fig. S5†). The further weight loss starts at about 300 °C which may be attributed to the decomposition of the framework of **1**.

The structure features of compound **1** indicate its potential application as a proton conductor. The short distances of O4W⋯O5W (2.67 Å) and O5W⋯O6W (2.73 Å) indicate strong hydrogen-bonding interactions between them. All the proton conductivities were evaluated by alternating current impedance spectroscopy. The bulk conductivity was assessed by semicircle fittings of the Nyquist plots. The conductivities of **1** were firstly measured under different relative humidity values at 30 °C. The results show that the conductivities rise from 4.6×10^{-8} S cm^{-1} at 80% RH to 3.1×10^{-5} S cm^{-1} at 98% RH (Fig. 4a), which indicates that high humidity is important for the conductivity while the water molecules in the channel of **1** not only can help complete the proton conducting pathways but also can act as proton carriers. The water vapour absorption and desorption isotherms of compound **1** confirm that its channels are accessible to water molecules (Fig. S6†). The temperature effects were also investigated at 98% RH. As the temperature rose, the conductivities increased to 1.4×10^{-4} S cm^{-1} at 65 °C from 3.1×10^{-5} S cm^{-1} at 30 °C (Fig. 4b). The Arrhenius plots of **1** were obtained as shown in Fig. 4d and the activation energy (E_a) was calculated to be 0.42 V at 98% RH. According to previous reports, the E_a values in the range of 0.1–0.4 eV or over 0.4 eV indicate that the proton

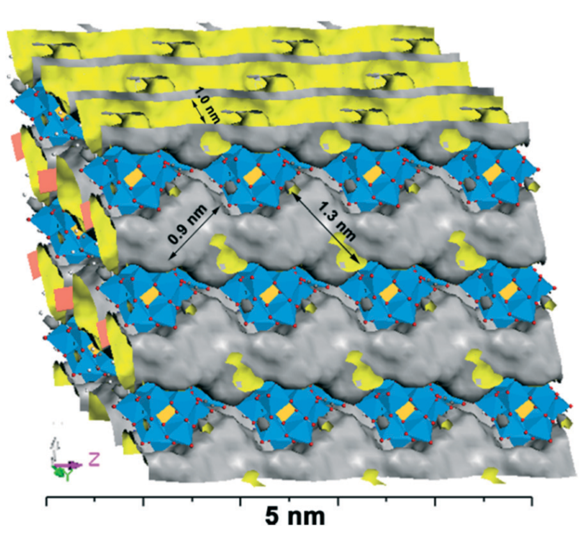

Fig. 2 Representation of 1D gourd-shaped channels of **1**. Yellow represents inside surfaces.

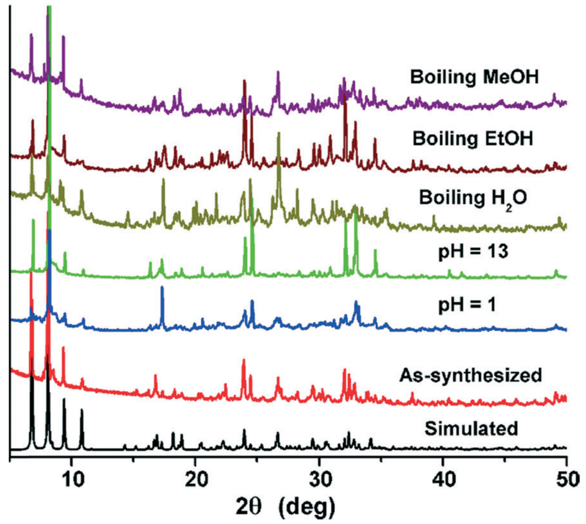

Fig. 3 PXRD patterns of **1** after being treated under different conditions.

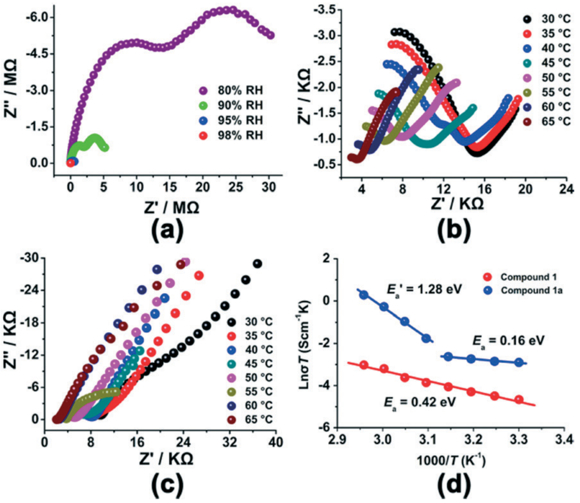

Fig. 4 (a) Impedance spectrum of **1** at 30 °C with different RH values. (b) Impedance spectrum of **1** under 98% RH at different temperatures. (c) Impedance spectrum of **1a** under 98% RH at different temperatures. (d) Arrhenius plots of proton conductivity for **1** and **1a** at 98% RH.

conducting process occurs through the Grotthuss mechanism or the vehicle mechanism, respectively.[10,31] As compound **1** shows an E_a value of 0.42 eV, the proton-conducting processes may occur through the vehicle mechanism.

In order to further improve the conductivity of compound **1**, we have modified its channel environment with $N_2H_4 \cdot H_2SO_4$. Here we take $N_2H_4 \cdot H_2SO_4$ in consideration for these reasons. Firstly, $N_2H_6^{2+}$ is one type of proton source as well as a good proton carrier.[32] Secondly, SO_4^{2-} could connect with SiW_{12} ions and water molecules by hydrogen bonds to generate more proton-transport pathways.[33–35] Thirdly, the void space in the framework of **1** is large enough for loading small $N_2H_6^{2+}$ and SO_4^{2-} ions. The $N_2H_4 \cdot H_2SO_4$ solution (0.1 mol L^{-1}, 20 ml) containing crystals of **1** (150 mg) is kept in an oven at 60 °C for 12 hours, then the microcrystalline powders are filtered out and washed thoroughly with deionized water to obtain **1a**. The colour of the sample changed from blue to cyan during the immersing process. The PXRD patterns reveal that the framework of **1a** remains intact (Fig. S8†). The FT-IR data confirm the successful loading of $N_2H_4 \cdot H_2SO_4$ (Fig. S9†). EA and TGA reveal that the loading of $N_2H_4 \cdot H_2SO_4$ was about 5.4 per unit cell (Fig. S9†). The conductivities of **1a** are also closely related to humidity, as they rise from 1.6×10^{-8} S cm^{-1} at 90% RH and 30 °C to 1.8×10^{-4} S cm^{-1} at 98% RH and 30 °C (Fig. S10†). The temperature dependence is also investigated at 98% RH, and the conductivities rise from 1.8×10^{-4} S cm^{-1} at 30 °C to 3.9×10^{-3} S cm^{-1} at 65 °C (Fig. 4c). It is noteworthy that the proton conductivity of **1a** at 65 °C and 98% RH is 28 times higher than that of compound **1**. The conductivity value of **1a** at 65 °C and 98% RH is comparable to the highest conductivity values that have been reported for POM-based coordination polymers (Table S3†).[22] The E_a values of **1a** from the Arrhenius plots were calculated to be 0.16 V between 30–45 °C and 1.28 eV between 50–65 °C at 98% RH, respectively. The results indicate that the proton-conducting processes in **1a** proceed through the Grotthuss mechanism below 45 °C and through the vehicle mechanism above 50 °C. The low E_a value of **1a** below 45 °C may be attributed to the introduction of $N_2H_6^{2+}$ and SO_4^{2-} ions, which are fixed in the hydrogen-bond networks and can help to improve the smoothness of these networks. When the temperature is increased up to 50 °C, the mobility of proton carriers such as water molecules and $N_2H_6^{2+}$ ions is improved, and thus they can move in the narrow channels but with a high energy barrier.

Conclusions

In summary, a new stable pillar-layered supramolecular CP, namely, $[Cu_4L_2(SiW_{12}O_{40})(OH)_4(H_2O)_8] \cdot 8H_2O$ (**1**), has been prepared by a hydrothermal method. The 1D gourd-shaped channels of **1** can be modified by $N_2H_4 \cdot H_2SO_4$, which not only can act as a proton carrier but also can help to improve the smoothness of the hydrogen-bond networks inside the solids, to generate **1a**. More importantly, compared to **1**, the proton conductivity of **1a** shows a 28-fold enhancement. These results present an efficient way to prepare highly proton-conducting materials through introducing $N_2H_6^{2+}$ and/or SO_4^{2-} ions into the channels of POM-based CPs.

Conflicts of interest

There are no conflicts to declare.

Acknowledgements

We gratefully acknowledge financial support from the National Natural Science Foundation of China (No. 21622104, 21371099, 21701084 and 21471080), the Natural Science Foundation of Jiangsu Province (No. BK20141445), the University Science Research Project of Jiangsu Province (16KJB150004), the China Postdoctoral Science Foundation (No. 2016M591875) and the Postdoctoral Science Foundation of Jiangsu Province (No. 1601239C).

References

1 H. Zhang and P. K. Shen, *Chem. Rev.*, 2012, **112**, 2780–2832.
2 L. Malavasi, C. A. J. Fisher and M. S. Islam, *Chem. Soc. Rev.*, 2010, **39**, 4370–4387.
3 R. F. Service, *Science*, 2002, **296**, 1222–1224.
4 M. Yoon, K. Suh, S. Natarajan and K. Kim, *Angew. Chem., Int. Ed.*, 2013, 52, 2688–2700.
5 S. L. Li and Q. Xu, *Energy Environ. Sci.*, 2013, **6**, 1656–1683.
6 Q. Li, R. He, J. O. Jensen and N. J. Bjerrum, *Chem. Mater.*, 2003, **15**, 4896–4915.
7 X. Meng, H. N. Wang, S. Y. Song and H. J. Zhang, *Chem. Soc. Rev.*, 2017, **46**, 464–480.
8 P. Ramaswamy, N. E. Wong and G. K. H. Shimizu, *Chem. Soc. Rev.*, 2014, **43**, 5913–5932.

9 S. S. Bao, G. K. H. Shimizu and L. M. Zheng, *Coord. Chem. Rev.*, 2018, DOI: 10.1016/j.ccr.2017.11.029.

10 T. Yamada, K. Otsubo, R. Makiura and H. Kitagawa, *Chem. Soc. Rev.*, 2013, **42**, 6655–6669.

11 M. T. Colomer, *Adv. Mater.*, 2006, **18**, 371–374.

12 Y. Ye, W. Guo, L. Wang, Z. Li, Z. Song, J. Chen, Z. Zhang, S. Xiang and B. Chen, *J. Am. Chem. Soc.*, 2017, **139**, 15604–15607.

13 F. M. Zhang, L. Z. Dong, J. S. Qin, W. Guan, J. Liu, S. L. Li, M. Lu, Y. Q. Lan, Z. M. Su and H. C. Zhou, *J. Am. Chem. Soc.*, 2017, **139**, 6183–6189.

14 N. E. Wong, P. Ramaswamy, A. S. Lee, B. S. Gelfand, K. J. Bladek, J. M. Taylor, D. M. Spasyuk and G. K. H. Shimizu, *J. Am. Chem. Soc.*, 2017, **139**, 14676–14683.

15 Y. S. Wei, X. P. Hu, Z. Han, X. Y. Dong, S. Q. Zang and T. C. W. Mak, *J. Am. Chem. Soc.*, 2017, **139**, 3505–3512.

16 S. S. Nagarkar, S. Horike, T. Itakura, B. Le Ouay, A. Demessence, M. Tsujimoto and S. Kitagawa, *Angew. Chem., Int. Ed.*, 2017, **56**, 4976–4981.

17 R. Li, S. H. Wang, X. X. Chen, J. Lu, Z. H. Fu, Y. Li, G. Xu, F. K. Zheng and G. C. Guo, *Chem. Mater.*, 2017, **29**, 2321–2331.

18 M. T. Pope, *Heteropoly and isopoly-oxometalates*, Springer-Verlag, Berlin, 1983.

19 E. L. Zhou, C. Qin, P. Huang, X. L. Wang, W. C. Chen, K. Z. Shao and Z. M. Su, *Chem. – Eur. J.*, 2015, **21**, 11894–11898.

20 H. Ma, B. Liu, B. Li, L. Zhang, Y. G. Li, H. Q. Tan, H. Y. Zang and G. Zhu, *J. Am. Chem. Soc.*, 2016, **138**, 5897–5903.

21 X. Lai, Y. Liu, G. Yang, S. Liu, Z. Shi, Y. Lu, F. Luo and S. Liu, *J. Mater. Chem. A*, 2017, **5**, 9611–9617.

22 S. Uchida, R. Hosono, R. Eguchi, R. Kawahara, R. Osuga, J. N. Kondo, M. Hibino and N. Mizuno, *Phys. Chem. Chem. Phys.*, 2017, **19**, 29077–29083.

23 J. Miao, Y. Liu, Q. Tang, D. He, G. Yang, Z. Shi, S. Liu and Q. Wu, *Dalton Trans.*, 2014, **43**, 14749–14755.

24 C. Dey, T. Kundu and R. Banerjee, *Chem. Commun.*, 2012, **48**, 266–268.

25 M. J. Janik, R. J. Davis and M. Neurock, *J. Am. Chem. Soc.*, 2005, **127**, 5238–5245.

26 Y. Zhou, J. Yang, H. Su, J. Zeng, S. P. Jiang and W. A. Goddard, *J. Am. Chem. Soc.*, 2014, **136**, 4954–4964.

27 X. L. Cao, S. L. Xie, S. L. Li, L. Z. Dong, J. Liu, X. X. Liu, W. B. Wang, Z. M. Su, W. Guan and Y. Q. Lan, *Chem. – Eur. J.*, 2018, **10**, 2365–2369.

28 J. Li, X. L. Cao, Y. Y. Wang, S. R. Zhang, D. Y. Du, J. S. Qin, S. L. Li, Z. M. Su and Y. Q. Lan, *Chem. – Eur. J.*, 2016, **22**, 9299–9304.

29 G. Sheldrick, *Acta Crystallogr., Sect. C: Struct. Chem.*, 2015, **71**, 3–8.

30 A. Spek, *Acta Crystallogr., Sect. D: Biol. Crystallogr.*, 2009, **65**, 148–155.

31 T. K. O. Nakamura, I. Ogino and Y. Miyake, *Chem. Lett.*, 1979, **8**, 17–18.

32 M. Sadakiyo, T. Yamada and H. Kitagawa, *J. Am. Chem. Soc.*, 2014, **136**, 13166–13169.

33 F. Yang, G. Xu, Y. Dou, B. Wang, H. Zhang, H. Wu, W. Zhou, J.-R. Li and B. Chen, *Nat. Energy*, 2017, **2**, 877–883.

34 S. Fujita, A. Koiwai, M. Kawasumi and S. Inagaki, *Chem. Mater.*, 2013, **25**, 1584–1591.

35 X. M. Li, L. Z. Dong, S. L. Li, G. Xu, J. Liu, F. M. Zhang, L. S. Lu and Y. Q. Lan, *ACS Energy Lett.*, 2017, **2**, 2313–2318.